

# MEASUREMENT OF SPECTRAL BREAKS IN PULSAR WIND NEBULAE WITH MILLIMETER-WAVE INTERFEROMETRY

D. C.-J. BOCK<sup>1</sup>

Radio Astronomy Laboratory, University of California, Berkeley, CA 94720

AND

B. M. GAENSLER

Harvard-Smithsonian Center for Astrophysics, 60 Garden Street MS-6, Cambridge, MA 02138

*Draft version September 23, 2018*

## ABSTRACT

We have observed pulsar wind nebulae in the three supernova remnants G11.2–0.3, G16.7+0.1, and G29.7–0.3 at 89 GHz with the Berkeley-Illinois-Maryland Association Array, measuring total flux densities of two of them for comparison with archival data at other frequencies. In G16.7+0.1, we find a break in the spectrum of the PWN at  $\sim 26$  GHz. In G29.7–0.3, our data suggest a break in the integrated spectrum of the central nebula at  $\sim 55$  GHz, lower than previously estimated. However, we have found spatial structure in the spectrum of this nebula. The emission to the north of pulsar J1846–0258 has a broken spectrum, with break frequency  $\lesssim 100$  GHz, consistent with a conventional pulsar-powered nebula. The emission to the south of the pulsar has a near-power-law spectrum from radio to X-rays: this component may be unrelated to the PWN, or may be evidence of asymmetries and/or time evolution in the pulsar’s energy output. We present 89 GHz images of each remnant.

*Subject headings:* pulsars: individual (J1846 – 0258)—radio continuum: ISM—SNR: individual (G11.2–0.3, G16.7+0.1, G29.7–0.3)—supernova remnants

## 1. INTRODUCTION

Pulsars are born spinning with up to  $10^{51}$  erg of rotational kinetic energy — as much energy as in the supernovae in which they are born. This vast reservoir of energy is ultimately deposited into the ambient medium through the pulsar’s relativistic wind. In many cases, this interaction between the pulsar and its environment is directly observable, in the form of a synchrotron-emitting pulsar wind nebula (PWN), of which the Crab Nebula is the best-known example. While many pulsars have their beams directed away from us, PWNe radiate isotropically. Thus PWNe are powerful probes of pulsars and their energy loss, even when the pulsar itself cannot be detected.

At radio frequencies, PWNe typically have flat spectra  $-0.3 < \alpha < 0$  ( $S_\nu \propto \nu^\alpha$ ), but in the X-ray band we generally see  $\alpha < -1$ . It is therefore commonly presumed that PWNe have at least one spectral break at intermediate wavelengths. Such breaks are expected from theoretical considerations, and result from a combination of synchrotron losses and the time-evolution of the pulsar’s changing energy output (Pacini & Salvati 1973; Reynolds & Chevalier 1984; Woltjer et al. 1997). Locating these breaks gives insight into the physical conditions of the pulsar wind: in PWNe powered by young ( $< 5$  kyr) pulsars, the spectral break can be used to infer directly the nebular magnetic field strength (e.g. Manchester, Staveley-Smith, & Kesteven 1993), while spatial variations in the break energy can be used to identify and map out the processes of particle diffusion and radiative losses within the flow (Amato et al. 2000; Bock, Wright, & Dickel 2001).

Most flux density measurements of PWNe to date have been in the X-ray and low-frequency radio bands. To pin down the break frequencies it is necessary to measure flux densities in the part of the spectrum near the spectral breaks, i.e. at millimeter and infrared wavelengths.

Here we report on observations of three PWNe for which extant data at radio and X-ray wavelengths implied a spectral break in or below the mm band. The PWNe, in the supernova remnants G11.2–0.3, G16.7+0.1, and G29.7–0.3 (Kesteven 75), were identified from the catalog of Green (2004) as being sufficiently bright and compact to allow imaging with millimeter interferometers. Two of the PWNe (in G11.2–0.3 and G29.7–0.3) contain young X-ray pulsars (Torii et al. 1997; Gotthelf et al. 2000). Only a few PWNe have been reliably imaged at millimeter wavelengths with single dish telescopes, and prior to this study only one (G21.5–0.9; Bock et al. 2001) had been imaged with a millimeter interferometer.

We have been able reliably to image two of the sources observed (in the supernova remnants G16.7+0.1 and G29.7–0.3), obtaining their total flux densities at 89 GHz. This has allowed us to determine the frequency of their spectral breaks at radio wavelengths using archival data and assuming the presence of a solitary break. We have been able to resolve the PWN in G29.7–0.3, letting us compare the millimeter-wave structure of the PWN with that in the X-ray band and at lower radio frequencies. We also present a millimeter-wave image of the SNR G11.2–0.3, which has a PWN with radio spectral index  $\alpha = -0.25_{-0.10}^{+0.05}$  (Tam, Roberts, & Kaspi 2002). However, its extension compared to the spatial sensitivity of the array precludes any quantitative analysis.

Electronic address: dbock@astro.berkeley.edu

Electronic address: bgaensler@cfa.harvard.edu

<sup>1</sup> present address: CARMA, P.O. Box 968, Big Pine, CA 93513

## 2. OBSERVATIONS

Observations were obtained at 88.6 GHz using the BIMA Array<sup>2</sup> (Welch et al. 1996) during 2002 and 2003 (Table 1). To achieve suitable  $uv$  coverage, we used the technique of multi-frequency synthesis over both 800 MHz sidebands of the local oscillator. We measured only the left circular polarization (in the sense of IEEE 1969) in the assumption that circularly polarized emission from the sources would be negligible.<sup>3</sup> In order to image fully the extended structure, and to assist with the recovery of low spatial frequency information, we imaged each source with a 7-point hexagonal mosaic. The primary beam of the 6.1-m antennas is Gaussian with FWHM  $2'.13$ . The short interferometer spacings (as low as 6.1 m when antennas are nearly shadowed) available from the array provide significant sensitivity on spatial scales up to an arcminute. The shortest physical baselines are 8.1 m.

The bright quasars QSO B1730–130 (for G11.2–0.3 and G16.7+0.1) and QSO B1741-038 (for G29.7–0.3) were observed as phase calibrators at 25 to 30 minute intervals, after 3 complete cycles of 7 pointings. We expect the astrometric accuracy of the images to be better than 1 arcsec, a precision routinely obtained with the BIMA Array (Looney & Hardcastle 2000). Single sideband system temperatures during the observations were between 200 and 600 K (scaled to outside the atmosphere). We used the on-line absolute flux density scale determined from many observations of planets, which have been found on average to be stable over time (Muhleman & Berge 1991). As a check we observed Uranus for 10 minutes during each observing session, finding a day-to-day scatter for the mean gain on all antennas between 0.95 and 1.12, implying multiplicative corrections to the flux density scale of between 0.91 and 1.25. The mean correction would be 1.09 for observations of G16.7+0.1 and 1.05 for G29.7–0.3. The gains for each sideband were consistent within a few percent on each day. In this paper we retain the on-line scale, and note that with several days' observations contributing to each image our measurements are consistent with an uncertainty in the overall flux density scale of about 10%.

Imaging was done with the MIRIAD software package (Sault, Teuben, & Wright 1995), using SDI deconvolution (Steer, Dewdney, & Itoh 1984): such CLEAN-based algorithms are generally superior to maximum entropy methods for low signal to noise ratios (Helfer et al. 2003). The multiple pointing centers were combined into a mosaiced image corrected for the primary beam. To assess the reliability of flux density recovery when imaging these sources, simulations of each observation were made with MIRIAD, using the actual observations as a template. The results of the simulations are presented with the data on each source in the next section.

## 3. RESULTS

<sup>2</sup> The BIMA Array was operated until June 2004 by the Berkeley-Illinois-Maryland Association with support from the National Science Foundation.

<sup>3</sup> The BIMA Array natively measured one linear polarization. To convert to circular polarization, 90-GHz quarter-wave plates were used.

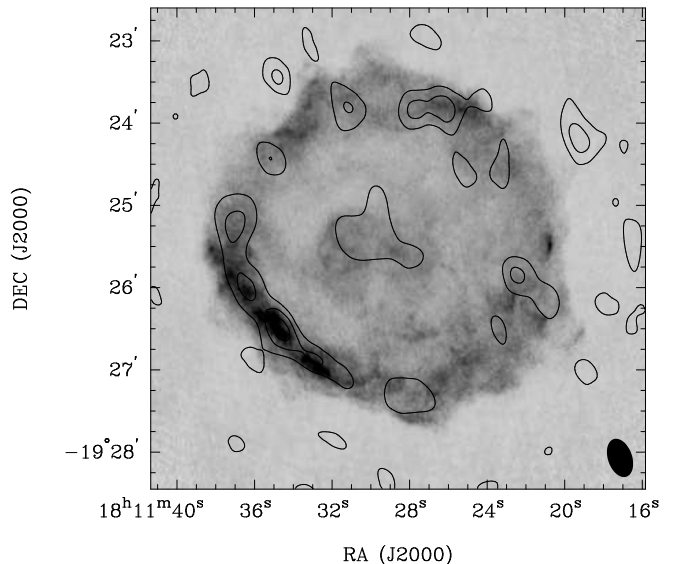


FIG. 1.— Image of G11.2–0.3 at 89 GHz (contours) and 8.6 GHz (grayscale; Roberts et al. 2003). The contours are at 10, 20, and 30 mJy beam<sup>-1</sup>. The synthesized beam at 89 GHz is shown at the lower right.

## 3.1. G11.2–0.3

The BIMA image of G11.2–0.3 is shown with contours in Figure 1, overlaid upon an 8.6 GHz image of Roberts et al. (2003). Based on positional coincidence with the 8.6 GHz emission, we appear to have detected the PWN in this remnant (the single contour at the center of the image). However, the extended structure in the PWN is not well imaged by the array: the modeling described in section 2 showed that we have measured only approximately 10% of the emission, indicating that the PWN is nearly resolved out on all baselines. Given the magnitude and unreliability of the correction factor required to estimate the true flux density, we do not believe that these data can provide a reliable estimate of the flux density of the PWN. High sensitivity single dish measurements would be required to investigate this object further.

## 3.2. G16.7+0.1

The PWN in this remnant (Figure 2) is detected as a peak of 14 mJy beam<sup>-1</sup> at  $8^{\text{h}}20^{\text{m}}57^{\text{s}}.2 -14^{\circ}19'34''$  (J2000). The feature is extended: an elliptical Gaussian fitted to the feature has a size of  $51'' \times 20''$  (at position angle  $6^{\circ}$  east of north), and an integrated flux density of 27 mJy. The size and position are consistent with the measurements of Helfand et al. (1989).

To assess the reliability of this measurement we have modeled the response of the array to two simple sources: a  $25'' \times 7''$  Gaussian with major axis  $10^{\circ}$  west of north and a  $45'' \times 15''$  Gaussian with major axis  $20^{\circ}$  west of north, corresponding approximately to the 50% and 20% contours in the 2 cm image of Helfand et al. (1989). In deconvolved images we recovered 97% and 80% of the total emission respectively, without taking into account a small residual negative background. We conclude that we should have measured at least 90% of the emission from this object, and consider that we have reliably determined the flux density of the PWN at this frequency.

TABLE 1  
SUMMARY OF OBSERVATIONS

SNR	Antenna Config.	Date(s)	Time on Source (hr)	Image rms (mJy beam <sup>-1</sup> )	Synthesized Beam	
					FWHM size (")	PA (°)
G11.2–0.3	D	2002 Jun 10	3.7	$\lesssim 10^a$	18.9×17.6	19.0
G16.7+0.1	D	2002 Jun 2, Sep 10; 2003 Sep 1,4	14.3	4	25.2×18.7	9.7
G29.7–0.3	D	2002 May 30, 2003 Aug 31	8.2	1.7 <sup>b</sup>	13.3×10.4 <sup>b</sup>	17.1 <sup>b</sup>
	C	2002 May 9,16	7.9			
	B	2002 Mar 15	5.6			

<sup>a</sup>Low-level emission throughout the field makes the rms difficult to determine accurately

<sup>b</sup>For C and D configuration observations

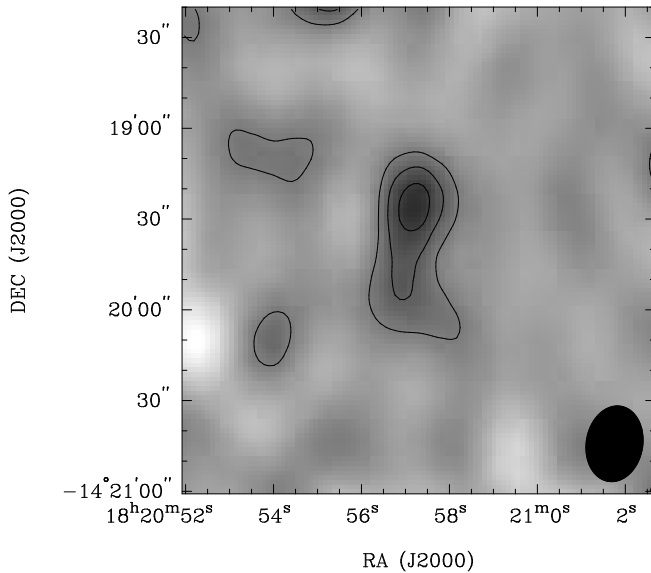


FIG. 2.— Image of G16.7+0.1 at 89 GHz. The contours are at 4, 8, and 12 mJy beam<sup>-1</sup>. The synthesized beam at 89 GHz is shown at the lower right.

Taking into account the uncertainty in the flux density scale (§2) and the low signal to noise we estimate the total uncertainty in our measurement to be no more than 20%.

### 3.3. G29.7–0.3 (Kesteven 75)

The BIMA image of G29.7–0.3 is presented in Figure 3. For comparison, the 1.4 GHz image of Helfand, Collins, & Gotthelf (2003b) is shown also. This object is sufficiently bright at millimeter wavelengths that we have been able to image it using both the BIMA C and D configurations. However, the data obtained with the B configuration did not add significantly to the results: they have not been included in the image in Figure 3, nor in the quantitative analysis that follows. In the figure, both the PWN (at the image center) and the partial shell (to the south and east) can easily be seen at each frequency. As expected, the PWN is relatively brighter than the shell at the higher frequency, i.e. it has a flatter spectral index. Note that the PWN is central in the corresponding X-ray image (Helfand et al. 2003b), which also shows the northern extent of the SNR’s shell.

We have measured an 89 GHz flux density for the PWN

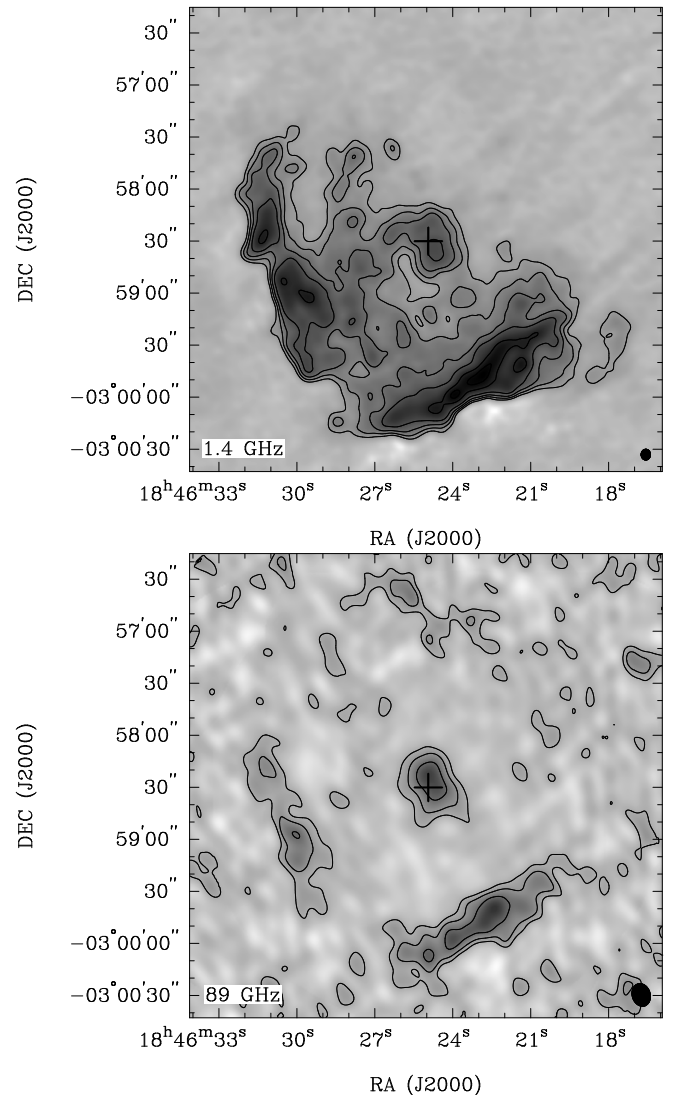


FIG. 3.— Images of G29.7–0.3 at 1.4 GHz (Helfand et al. 2003b; contours 2, 5, 10, 20, 50, 80 mJy beam<sup>-1</sup> on logarithmic grayscale) and 89 GHz (linear scale; contours at 2, 5, 10, 20 mJy beam<sup>-1</sup>). The position of the pulsar J1846–0258 (Gotthelf et al. 2000) is marked with a cross. The synthesized beams are shown at the lower right of each image.

of 80 mJy in  $0.6 \text{ arcmin}^2$  (within approximately the “0 mJy beam $^{-1}$  contour”), taking into account a local background (a “negative bowl”) within the SNR shell of about  $-36 \text{ mJy arcmin}^{-2}$ . To quantify the degree to which the array is sensitive to the extended emission, we simulated an observation of the PWN using the 1.4 GHz image (Helfand et al. 2003b) as a model.<sup>4</sup> We added Gaussian noise to the undeconvolved image to give a similar signal to noise ratio. After deconvolution, we recovered 92.4% of the flux density in the simulated observation. Applying the correction for interferometric filtering of the extended emission thus determined, we obtain a flux density for the PWN of 86 mJy. In the simulation the negative background was much less pronounced than in the BIMA observation: this artifact is thus probably due primarily to poor deconvolution of emission from the SNR shell, which was not included in our simulation. We consider an upper limit to the imaging errors to be 10%; combining this with the 10% flux calibration uncertainty (§2) leads to a total uncertainty of 15%.

At the nearby frequency of 84 GHz, the observations of Salter et al. (1989) imply an integrated flux density of 159 mJy, inconsistent with the present data. However, the earlier observations were made using a single dish with a beam of  $76'' \times 70''$ , substantially larger than the characteristic source size ( $\sim 30'' \times 20''$ ). Salter et al. corrected their measurement for the smaller source size to derive their integrated flux density. However, it seems possible that Salter et al. also measured some shell emission. The advantage of the present interferometric measurement is that it would have filtered out any contaminating emission from the SNR’s shell, and should provide a more reliable determination of the flux density attributable to the PWN alone.

#### 4. DISCUSSION

##### 4.1. G16.7+0.1

A spectrum of the PWN in G16.7+0.1 is shown in Figure 4. There are few measurements available of the flux density of this PWN. The solid line at low frequencies represents the radio spectrum derived from observations at 6, 20, and 90 cm by Helfand et al. (1989). Recent X-ray measurements (Helfand, Agüeros, & Gotthelf 2003a) imply that there must be at least one break between the radio and X-ray regimes; the present measurement implies that this is at about 26 GHz (central dotted line). In the figure, the gray shaded area represents the region of intersection of the Helfand et al. radio spectrum and a simple radio/X-ray spectrum (i.e. assuming a single break between X-ray and radio wavelength) consistent with the 89 GHz and X-ray uncertainties. This provides one way to quantify the uncertainty in the break frequency: the region has minimum and maximum frequencies (shown by the outer dotted lines) of 16 and 42 GHz respectively, leading to an estimate of the break frequency of  $26^{+16}_{-10}$  GHz.

The PWN in G16.7+0.1 has one of the lowest known break frequencies in a PWN: breaks at lower or comparable frequencies have been reported only in G27.8+0.6

<sup>4</sup> We chose this image for a model owing to its higher signal to noise. Recalling the flat PWN spectrum in the radio, we do not believe that the difference between the PWN shape at the two frequencies will significantly affect our result.

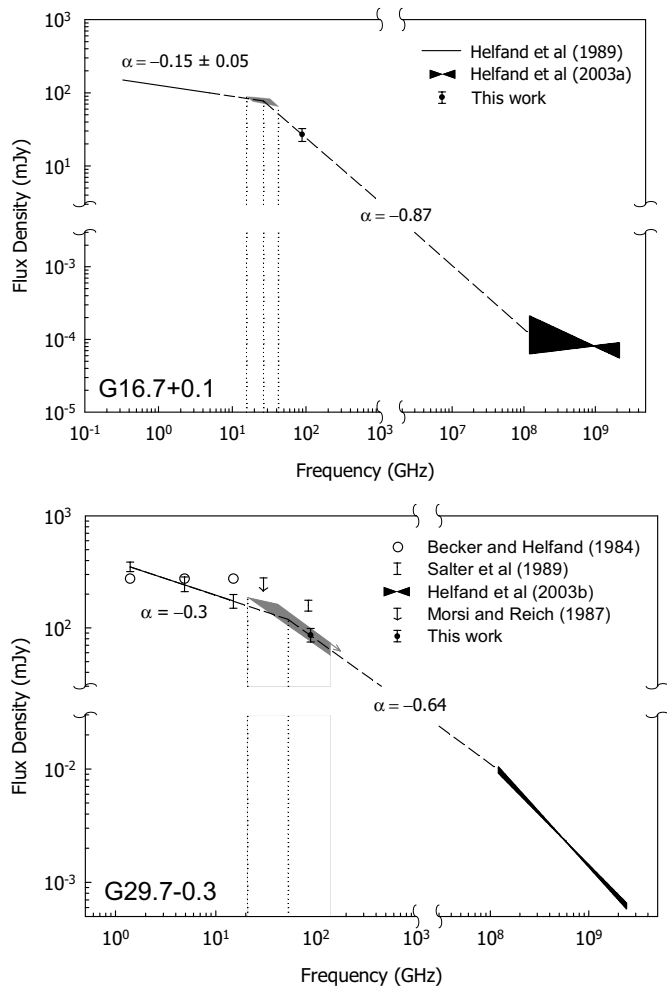


FIG. 4.— Integrated spectra of the pulsar wind nebulae in G16.7+0.1 and G29.7–0.3. In regions where the spectra are well determined they are shown with unbroken lines. Elsewhere simple straight line spectra implied by sparse measurements are shown by a dashed line. Uncertainties are shown where available; at X-ray wavelengths these are indicated by black shading. The regions within which spectral breaks are implied are shown by gray shading, and bounded by the vertical dotted lines (see text for details).

(between 5 and 10 GHz; Reich, Fürst, & Sofue 1984) and G74.9+1.2 (between 10 and 30 GHz; Morsi & Reich 1987a). Surprisingly, the spectrum within the X-ray band ( $\alpha = -0.17 \pm 0.29$ ) is flatter than the radio to X-ray spectrum. Presumably this is not the result of inverse Compton scattering, which is generally expected to be significant at  $\gamma$ -ray wavelengths. This phenomenon has been seen in one other PWN, that around the pulsar PSR B1757–24 (Kaspi et al. 2001).<sup>5</sup> In that case, the X-ray and radio spectra are also approximately flat, with a steeper spectrum required to connect the radio and X-ray observations. However, whereas Kaspi et al. found that the X-ray spectrum was just marginally consistent with the implied radio to X-ray average spectrum, this possibility is very unlikely in the case of G16.7+0.1, where the average radio to X-ray spectrum is not consistent with

<sup>5</sup> A step like that in the spectrum of the Crab Nebula at infrared/optical wavelengths, thought due to dust reradiation or extinction (Manchester & Taylor 1977), would not show up in the bulk radio to X-ray spectral index in the same way.

the X-ray data even within the 90% uncertainty limits of Helfand et al. (2003a).

One explanation for spectra of this shape is given by Reynolds & Chevalier (1984). They calculate that a combination of older particles suffering synchrotron losses due to compression of the magnetic field by the reverse shock and particles injected after the shock can give rise to a spectrum of this shape. However, whereas the reserve shock is expected to arrive after about  $10^4$  years, Helfand et al. (2003a) have estimated G16.7+0.1 to be only about 2000 years old. Therefore this seems like an unlikely explanation for this source.

#### 4.2. *G29.7–0.3: Integrated Spectrum of the PWN*

An integrated spectrum of the central nebula in G29.7–0.3 is plotted in Figure 4. This object was first seen by Becker & Kundu (1976), who measured a radio spectral index of  $-0.27$ , flatter than that of the SNR shell. VLA observations (Becker & Helfand 1984) confirmed the discovery but implied a flat ( $\alpha = 0.0$ ) spectrum. Hunt et al. (as reported by Salter et al. 1989) from different VLA observations obtained integrated flux density measurements that imply a radio spectral index of  $-0.30$ . Both sets of VLA observations are plotted in Figure 4. We have measured a flux density of 343 mJy for the PWN in the recent 1.4 GHz data of Helfand et al. (2003b), consistent with the Salter et al. result.

At higher frequencies, Morsi & Reich (1987b) measured 0.28 Jy from the PWN at 30 GHz, but note that they could have suffered from confusion (their observations had resolution  $26''.5$ ), leading to an overestimated result. It seems possible that they measured some of the broad underlying shell-related emission as well, which was not imaged at 89 GHz, and could have been poorly imaged at lower radio frequencies. This could have led to a further overestimate. As noted earlier (§3.3) we consider the Salter et al. 84 GHz measurement also to be an overestimate, for similar reasons.

Combined with the Salter et al. lower-frequency measurements, the X-ray data of Helfand et al. (2003b), and assuming a simple unbroken spectrum between radio and X-ray wavelengths, our observations imply a spectral break at approximately 55 GHz (shown by the right-hand vertical dotted line in the figure). Assuming the break to be sharp, the integrated flux density of the PWN at this frequency would be about  $120 \text{ mJy beam}^{-1}$ . Allowing the spectrum above and below the putative break to vary within the uncertainties of the measurements implies that the break should fall within the shaded gray area, with a minimum frequency of 21 GHz (left-hand vertical line). The break is not strictly constrained at high frequencies, since a straight line is just consistent with the low-frequency Hunt et al. measurements and our 89 GHz measurement. However, it is likely that the break is below 89 GHz.

We could alternatively have used the centimeter-wave data of Becker & Helfand (1984) and obtained a somewhat lower break frequency. However, given the agreement between the data of Salter et al. and Helfand et al. (2003b), and the fact that the Salter et al. data were quoted with uncertainties, we prefer the later measurements.

#### 4.3. *G29.7–0.3: Lobes of the PWN?*

The high resolution X-ray data clearly show two lobes of emission, to the north and south of the pulsar. The northern lobe is brighter at X-ray wavelengths. A comparison of images of the PWN at 1.4 GHz, 89 GHz and in X-rays (Figure 5) reveals that the PWN spectrum is also asymmetric. At 1.4 GHz, the PWN is brighter south of the pulsar, while at 89 GHz and above it is brighter north of the pulsar. These two components may have different origins, causing an integrated spectrum to be difficult to interpret.

In Table 2, we show flux densities of these northern and southern lobes, integrated over the regions shown in Figure 5. The regions chosen were a compromise between the competing desires to minimize contamination from the background and to include the majority of emission at each frequency. The area around the pulsar was excluded from all datasets, avoiding the need to estimate an X-ray background for normalizing the integrated areas. At 89 GHz the same background as in §2 was subtracted. Helfand et al. (2003b) were not able to find a significant difference between the X-ray spectra of the northern and southern lobes, so the X-ray flux densities quoted correspond to the luminosity reported by Helfand et al., apportioned according to the total counts in the two regions, assuming a uniform X-ray spectrum across the PWN. The 89 GHz uncertainties quoted are as in section 2, those for X-rays are the standard errors for a Poisson distribution, and we assign an uncertainty of 10% to the 1.4 GHz measurements, to account for imaging errors. This is probably an overestimate of the true uncertainty at 1.4 GHz.

Given the differing resolutions and systematic errors of the three datasets<sup>6</sup>, the results are necessarily qualitative. However, as may be seen in Figure 6, the northern lobe not only has a flatter spectrum on average, but shows strong evidence for break. Meanwhile, the spectrum of the southern lobe may be unbroken. In the figure, the uncertainties at radio frequencies are of order the point size, while those of the X-ray values are much smaller. The excellent positional agreement of the SNR shell at 1.4 and 89 GHz confirms the registration of the images. We believe that the difference in spectral shape between the lobes is reliable.

The same result may be obtained qualitatively by convolving the 1.4 GHz and X-ray observations to the resolution of the 89 GHz data (Figure 7). For this analysis, a background estimated at 24 counts/pixel was substituted for X-ray emission from the pulsar before convolution. From the figure, it is clear that the trend of steeper emission to the south holds. Although the systematic uncertainties are different, this method again implies a break in the spectrum of the northern lobe, and allows the southern lobe to have a simple power law spectrum from radio to X-rays.

The simplest explanation for the difference in spectrum to the north and south of the pulsar is that we are seeing both PWN and shell emission superimposed. In this scenario, a majority of the steep-spectrum emission seen at 1.4 GHz is attributed to the shell, seen near the pulsar due to projection. Other 1.4-GHz emission presumably from the shell may be seen at to the east of the

<sup>6</sup> In the 89 GHz image, there are only 3 beam areas within the northern region.

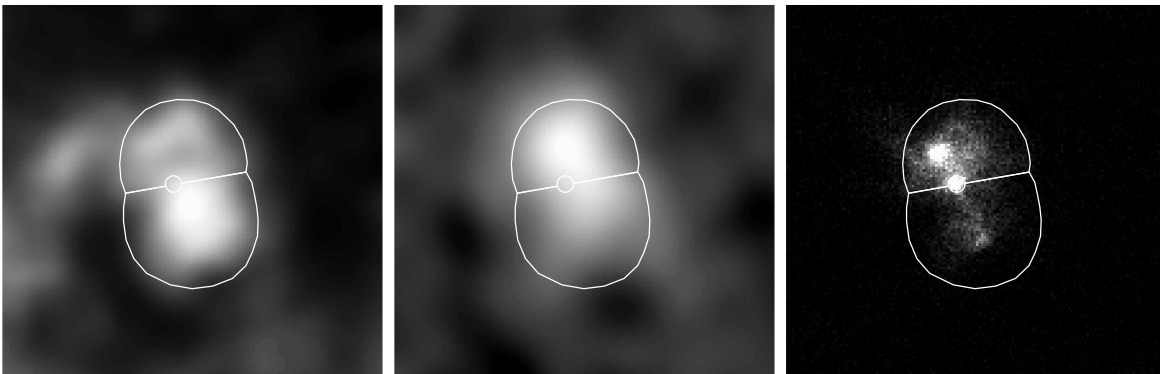


FIG. 5.— Images of G29.7–0.3 at (left to right) 1.4 GHz (Helfand et al. 2003b), 89 GHz, and 0.5–10 keV (*Chandra* archive; as presented by Helfand et al. 2003b), showing the regions over which emission was integrated in the southern and northern lobes.

TABLE 2  
FLUX DENSITIES OF THE LOBES AROUND THE PULSAR IN G29.7–0.3

Frequency (GHz)	Flux Density (uncertainty) (mJy)	
	N. lobe	S. lobe
1.4	170(35)	230(35)
89	34(5)	31(5)
$1.2 \times 10^8$ (0.5 keV)	0.00675(5)	0.00303(3)

NOTE. — Datasets for the measurements at 1.4 GHz and 0.5 keV are as referenced in Figure 5

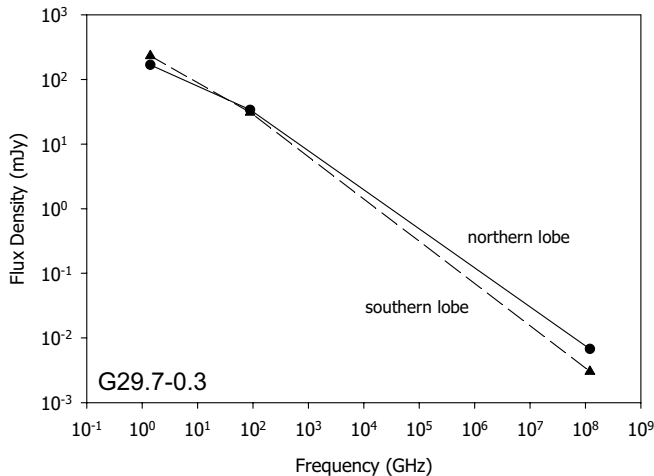


FIG. 6.— Simple “straight-line” spectra of the northern and southern lobes of the PWN in G29.7–0.3, derived from the data in Table 2.

PWN in Figure 3. The extent of the true PWN is then seen most easily in X-rays, where the southern portion is much fainter.

The asymmetry in the position of the pulsar with respect to the northern lobe (the implied true PWN) may be due to the passage of a reverse shock from the interaction of the supernova with the surrounding medium. An asymmetric medium will cause an asymmetric reverse shock. This phenomenon has been used to account for the PWN in the Vela supernova remnant, which is largely to one side of the presumed progenitor position

(Blondin, Chevalier, & Frierson 2001). However, the expected  $10^4$  years until the reverse shock is much larger than the age implied by the pulsar’s rate of spin down, which falls in the range  $\sim 700$ –1700 years (Gotthelf et al. 2000; Mereghetti et al. 2002). Thus in the absence of an extremely dense ISM the passage of a reverse shock does not seem a likely explanation for the asymmetry.

An alternative possibility is that the pulsar may have traveled from the apparent center of the PWN since the explosion. Assuming that the pulsar was born at the brightest part of the northern lobe, the kinematic distance of 21 kpc (Becker & Helfand 1984) and age range above imply a transverse velocity of 400–1000 km s<sup>−1</sup>. The upper end of this range is higher than the transverse velocity of almost all known pulsars, so improved pulsar timing (and eventually proper motion measurements) should allow us to evaluate this scenario in the future, although we note that this pulsar has so far been detected only in X-rays.

A final possibility is that the asymmetry in the nebula is intrinsic to the pulsar wind. In this case the southern lobe could be unassociated shell emission, as suggested above, or a part of the PWN with a different spectral shape.

#### 4.4. Origin of the Spectral Breaks

In both the PWNe in G16.7+0.1 and G29.7–0.3, there is strong evidence for a low frequency spectral break. For G29.7–0.3, this break may, as mentioned above, occur only in the northern lobe of the PWN. Both remnants are relatively youthful. The conventional spectral break due to synchrotron losses in a field  $B$  mG occurs at age  $\sim 40B^{-1.5}\nu^{-0.5}$  kyr at frequency  $\nu$  GHz. Thus

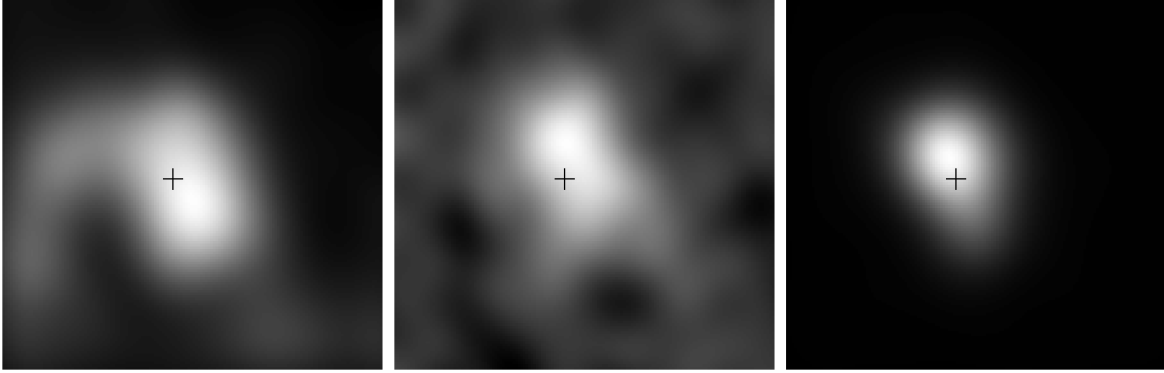


FIG. 7.— As for Figure 5, all convolved to the resolution of the 89 GHz image. The position of PSR J1846–0258 has been marked with a cross.

for G16.7+0.1 we expect a field of  $\sim 2.5$  mG, while for G29.7–0.3 we expect  $> 1.5$  mG. These values are substantially higher than inferred in other remnants from equipartition arguments, or more directly in the Crab Nebula (e.g. Hester et al. 1996), and seem to indicate that standard synchrotron losses alone are not the origin of the breaks.

We are left with the conclusion that perhaps these are indeed remnants of a “second kind” (Woltjer et al. 1997), in which intrinsic processes result in a spectrum different from that of the Crab. One possibility is that the pulsar’s excitation has decreased substantially at some point (Green & Scheuer 1992), with the break moving to lower frequencies with time (Woltjer et al. 1997). Alternatively the pulsar injection spectra may not be a simple power law.

## 5. CONCLUSIONS

We have carried out observations of three pulsar wind nebulae at millimeter wavelengths with the Berkeley-Illinois-Maryland Association Array. One of these PWNe, in the SNR G11.2–0.3, was not adequately imaged to allow quantitative analysis. We find the break frequency of the PWN in G16.7+0.1 to be at about 26 GHz, and see an unusual upturn in the spectrum below or in the X-ray band. In only one other PWN, that surrounding PSR B1757–24, has a similar effect been implied.

The bulk spectrum of the PWN in G29.7–0.3 indicates a likely spectral break at 55 GHz, but our observations and previous data reveal a marked variation in spectrum across the PWN. The spectrum is steeper to the south of the pulsar. It may be that the southern emission does not represent the continuing effect of the pulsar, but corresponds to a part of the SNR shell seen in projection. However, we cannot account for the one-sided PWN under this scenario.

The number of PWNe for which an analysis like this may be made is limited by the large size of the PWNe compared to the spatial scales on which millimeter interferometers are sensitive. However, the sensitivity and resolution of next generation instruments, such as ALMA, will allow these investigations to be conducted on much larger samples in other galaxies. Meanwhile, improved single-dish mapping techniques and sensitive wide-field imaging interferometers such as CARMA could enhance the high-frequency data on Galactic PWNe.

We thank E. Gotthelf, D. Helfand, and M. Roberts for making available their data in electronic form, and M. Wright for useful discussions. This work has made use of the NASA ADS and was partially supported by NSF grants AST-9981308 and AST-0228963 to the University of California, Berkeley.

## REFERENCES

- Amato, E., Salvati, M., Bandiera, R., Pacini, F., & Woltjer, L. 2000, *A&A*, 359, 1107
- Becker, R. H. & Helfand, D. J. 1984, *ApJ*, 283, 154
- Becker, R. H. & Kundu, M. R. 1976, *ApJ*, 204, 427
- Bock, D. C.-J., Wright, M. C. H., & Dickel, J. R. 2001, *ApJ*, 561, L203
- Blondin, J. M., Chevalier, R. A., & Frierson, D. M. 2001, *ApJ*, 563, 806
- Camilo, F., et al. 2002, *ApJ*, 571, L41
- Gaensler, B. M., van der Swaluw, E., Camilo, F., Kaspi, V. M., Baganoff, F. K., Yusef-Zadeh, F., & Manchester, R. N. 2004, *ApJ*, 616, 383
- Green D. A., 2004, *Bulletin of the Astronomical Society of India*, 32, 335
- Green, D., & Scheuer, P. 1992, *MNRAS*, 258, 943
- Gotthelf, E. V., Vasishth, G., Boylan-Kolchin, M., & Torii, K. 2000, *ApJ*, 542, L37
- Helfand, D. J., Agüeros, M. A., & Gotthelf, E. V. 2003a, *ApJ*, 592, 941
- Helfand, D. J., Collins, B. F., & Gotthelf, E. V., 2003b, *ApJ*, 582, 783
- Helfand, D. J., Velusamy, T., Becker, R. H., & Lockman, F. J. 1989, *ApJ*, 341, 151
- Helfer, T. T., Thornley, M. D., Regan, M. W., Wong, T., Sheth, K., Vogel, S. N., Blitz, L., & Bock, D. C.-J. 2003, *ApJS*, 145, 259
- Hester, J. J. et al. 1996, *ApJ*, 456, 225
- IEEE, 1969, *Standard Definitions of Terms for Radio Wave Propagation*, IEEE Trans. AP-17, 270-275
- Kaspi, V. M., Gotthelf, E. V., Gaensler, B. M., & Lyutikov, M. 2001, *ApJ*, 562, L163
- Looney, L. W. & Hardcastle, M. J. 2000, *ApJ*, 534, 172
- Manchester, R. N., Staveley-Smith, L., & Kesteven, M. J. 1993, *ApJ*, 411, 756
- Manchester, R. N., & Taylor, J. H. 1977, *Pulsars* (San Francisco: W. H. Freeman)
- Mereghetti, S., Bandiera, R., Bocchino, F., & Israel, G. L. 2002, *ApJ*, 574, 873
- Morsi, H. W. & Reich, W. 1987a, *A&AS*, 69, 533
- Morsi, H. W. & Reich, W. 1987b, *A&AS*, 71, 189

- Muhleman, D. O. & Berge, G. L. 1991, *Icarus*, 92, 263  
Pacini, F. & Salvati, M. 1973, *ApJ*, 186, 249  
Reich, W., Fürst, E., & Sofue, Y. 1984, *A&A*, 133, L4  
Reynolds, S. P. & Chanan, G. A. 1984, *ApJ*, 281, 673  
Reynolds, S. P. & Chevalier, R. A. 1984, *ApJ*, 278, 630  
Roberts, M. S. E., Tam, C. R., Kaspi, V. M., Lyutikov, M., Vasisht, G., Pivovarov, M., Gotthelf, E. V., & Kawai, N., 2003, *ApJ*, 588, 992  
Salter, C. J., Reynolds, S. P., Hogg, D. E., Payne, J. M., & Rhodes, P. J. 1989, *ApJ*, 338, 171  
Sault, R. J., Teuben, P. J., & Wright, M. C. H. 1995, in *ASP Conf. Ser. 77, Astronomical Data Analysis Software and Systems IV*, ed. R. A. Shaw, H. E. Payne, & J. J. E. Hayes (San Francisco: ASP), 433  
Steer, D. G., Dewdney, P. E., & Ito, M. R. 1984, *A&A*, 137, 159  
Tam, C., Roberts, M. S. E., & Kaspi, V. M. 2002, *ApJ*, 572, 202  
Torii, K., Tsunemi, H., Dotani, T., & Mitsuda, K. 1997, *ApJ*, 489, L145  
Welch, W. J. et al. 1996, *PASP*, 108, 93  
Woltjer, L., Salvati, M., Pacini, F., & Bandiera, R. 1997, *A&A*, 325, 295